2014 ITSS in Lyngby, Denmark

HARTNAGEL H. L., Darmstadt University of Technology
Merckstraße 25, D-64283 Darmstadt, Germany
Tel: +49(0)6151-16-2162
e-mail: hartnagel@mwe.tu-darmstadt.de
webaddress:http://www.mwe.tu-darmstadt.de

Review of Relevant Fundamentals for Latest Developments in Microwave and Optical Electronics.

1) Introduction.

Most of the present-day and future microwave and optical components for telecommunication and all the related subjects can only be understood on the basis of heterostructure engineering and quantum electronics. These concepts and some resulting devices and circuits are to be described by this lecture. The new device opportunities are often based on low-dimensional electronic structures.

A special feature is the new situation based on the opportunities of Nanometric Electronics. The design and assessment of the fabrication techniques have been studied.

2) Heterostructure Engineering.

An essential feature is the growth of single-crystal semiconducting layers on such substrates as Si or GaAs, either lattice matched or with a slightly mismatched lattice constant, as can be seen by Fig. 1, where the energy gap of this material is given as a function of lattice constant for the type of lattice relevant for this particular semiconductor (see also table 1). By combining two materials on top of each other with lattice matching by epitaxial technique we have to use such 2.

Fig 1. The bandgap of semiconductors as a function of their lattice constant**.**

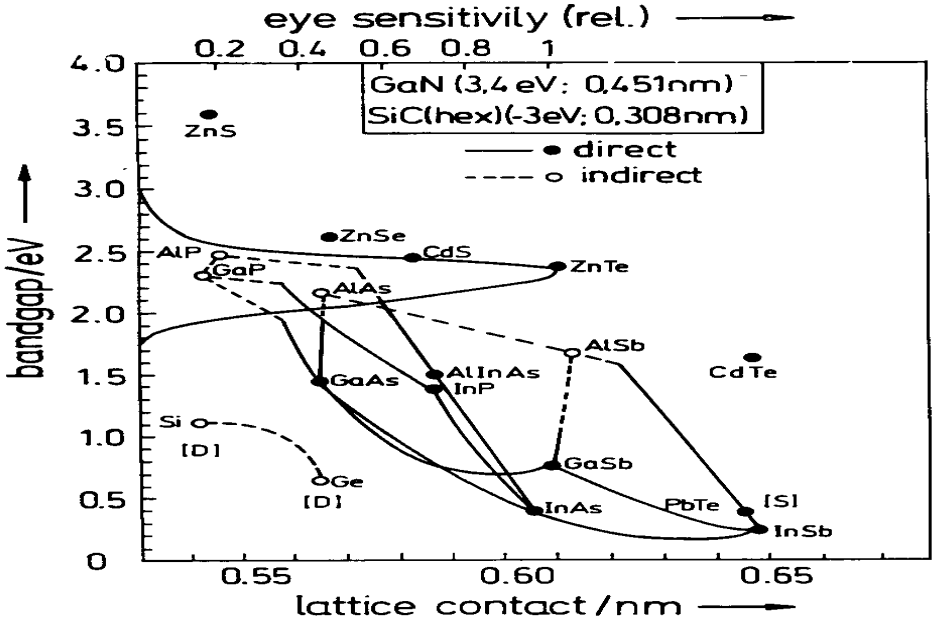

D - diamond lattice crystal
S - NaCl-type lattice
all others: zincblende lattice

Band gap and lattice data (T=300K)

Material	Lattice constant (Å)	$E_g(\Gamma)$ (eV)	$E_g(L)$ (eV)	$E_g(X)$ (eV)	Φ_{bv} (eV)
AlP	5.463 5	3.6	3.5[a]	2.45	1.27[a]
AlAs	5.660 5	3.00	2.36	2.15	1.002
AlSb	6.135 8	2.3	2.21	1.612	0.47
GaP	5.451 0	2.78	2.6	2.272	0.797
GaAs	5.653 25	1.424	1.708	1.900	0.562
GaSb	6.096 02	0.725	0.810	1.032	0.07
InP	5.868 9	1.350	1.95	2.15	0.857
InAs	6.058 3	0.355	1.43[a]	2.0[a]	0.58
InSb	6.479 43	0.170	1.0[a]	1.7	0.04
Si	5.431 1	4.1	2.0	1.124	0.447
Ge	5.657 9	0.805	0.666	0.89	0.072

[a] indicates theoretical estimate

Table 1. The lattice constant, the energy gaps of the Γ, L and X positions in the Brillouin zone and the activation energy ϕ_{bv},. necessary for electrons to leave the semiconductor.

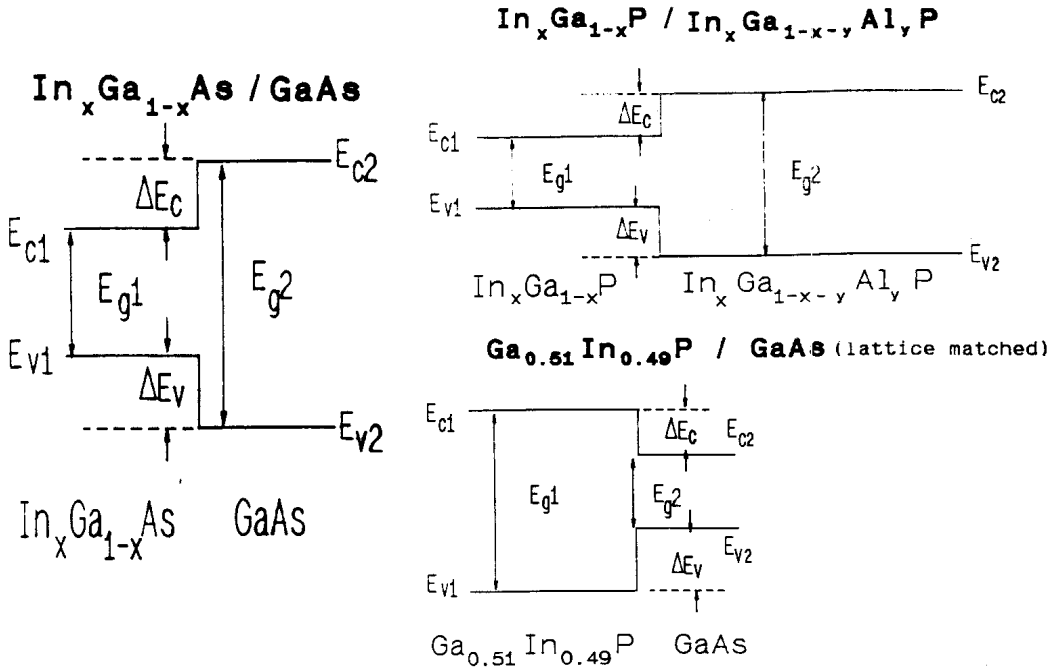

Fig. 2. Energy gap alignments for the transitions InGaAs/GaAs, InGaP/InGaAlP and GaInP/GaAs.

When such two different semiconducting materials meet each other, the transport properties are changed. Firstly, there is a change of energy gap. Then, the energy gaps are aligned to each other so that a conduction band offset ΔE_c and a valence band offset ΔE_v occurs, as shown by table 2, and for some examples, Figure 2.

Discontinuity references (T=300K)

Lattice constant of group (Å)	Material system	ΔE_g (eV)	ΔE_c (eV)	ΔE_v (eV)
5.44	GaP/Si	1.148	0.798	0.35
5.66	GaAs/Ge	0.758	0.268	0.49
	AlAs/Ge	1.48	0.55	0.93
	$Ga_{0.7}Al_{0.3}As/GaAs$	0.395	0.263	0.132
	AlAs/GaAs	0.73	0.29	0.44
	$Ga_{0.51}In_{0.49}P/GaAs$	0.463	0.223	0.24
5.87	$Al_{0.48}In_{0.52}As/InP$	0.106	0.30	−0.194
	$InP/Ga_{0.47}In_{0.53}As$	0.600	0.20	0.40
	$Al_{0.48}In_{0.52}As/Ga_{0.47}In_{0.53}As$	0.706	0.50	0.206
6.10	AlSb/GaSb	0.887	0.487	0.40
	GaSb/InAs	0.370	0.88	−0.51
	AlSb/InAs	1.257	1.367	−0.11

Table 2. The Change of energy gap ΔE_g, the conduction band offset ΔE_c and the valence band offset ΔE_v for a number of heterostructure transitions.

The concept of an energy gap is of course describing the charge carrier transport by a first approximation. In reality, the charge carriers are electron waves, for which the Schroedinger equation needs to be solved in the crystal lattice. This can be done in a representative cell called the Brillouin Zone, as given for normal semiconductor crystals by the upper part of Fig 3. Solving the Schroedinger equation gives then the energy contours in a Brillouin Zone whose coordinates are the wave vectors or, in other words, the momentum space and this is given for several examples by Fig. 4. Here, the separation of the minimum of the conduction band and of the maximum of the valence band gives the energy gap. If the maximum is at the same point as the minimum, one has a direct gap semiconductor, which can produce light by electron-hole recombination if, on the other hand, the minimum is at a different position than the maximum, one has an indirect semiconductor, where no photon emission is normally possible (see also details in Fig 1).

There are a number of special points in the Brillouin Zone, namely Γ, X und L. If we look for these points into Fig 4, we see that there are local valleys in the momentum space. At these points special effects such as the Gunn-effect oscillation can occur which are, however, here not explained in detail. If we mix the Ga/Al ratio in GaAlAs, then we can see from the lower part of Fig 3 how this changes the properties from direct-gap to indirect-gap material.

The slopes of the energy contours of Fig 4 give the effective masses of the charge carriers, as shown by table 3. The effective mass goes into the values of the low-field mobility.

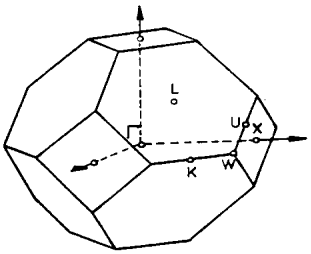

Erste Brillouinzone des fcc Gitters.

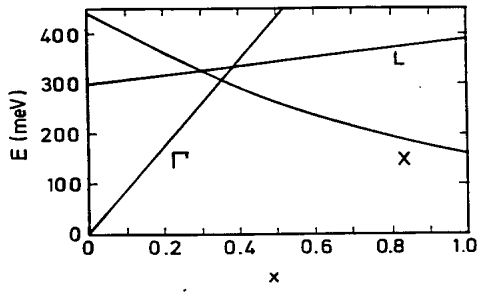

Energetischer Abstand der Leitungsbandminima zum Γ–Minimum in $Al_x Ga_{x-1} As$ als Funktion des Aluminiumgehaltes.

Fig 3: The upper part shows the Brillouin Zone of inverse space or wave vector space for the solution of the electron wave properties in such semiconductors as GaAs

The lower part shows the Γ-valley position, the X-valley position and the L-valley position above the valence band maximum as a function of the ratio Al/Ga = x for AlGas

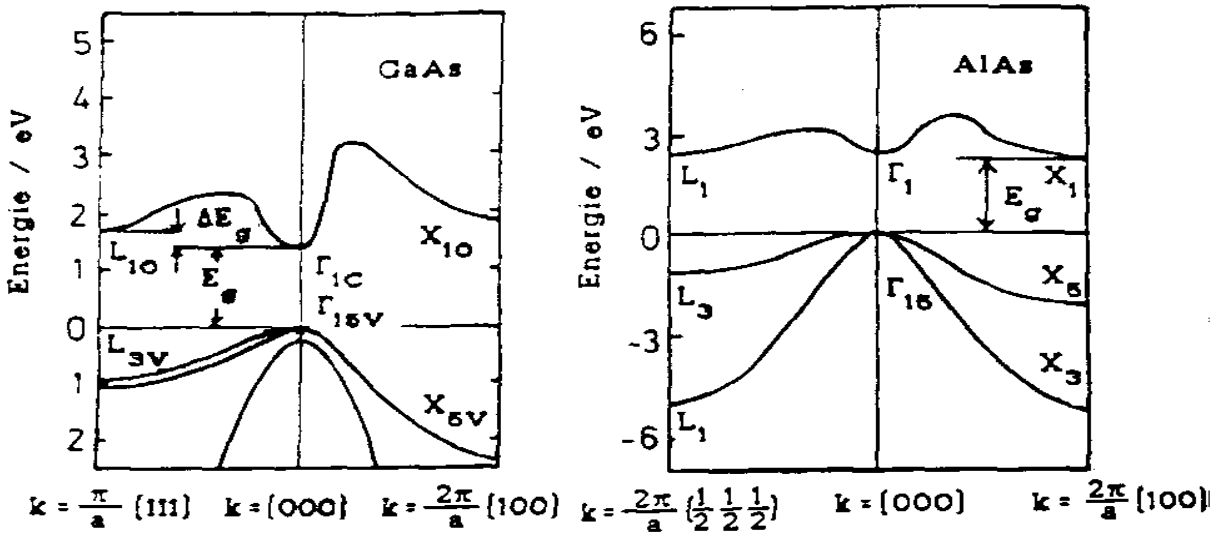

Bandstruktur von GaAs (links) und AlAs (rechts)

Fig 4. The solution of the wave function for GaAs (left) and AlAs (right) at the points Γ, X and L of the Brillouin Zone and intermediate positions.

Band gap and lattice data (T=300K)

Material	Lattice constant (Å)	$E_g(\Gamma)$ (eV)	$E_g(L)$ (eV)	$E_g(X)$ (eV)	Φ_{bv} (eV)
AlP	5.463 5	3.6	3.5[a]	2.45	1.27[a]
AlAs	5.660 5	3.00	2.36	2.15	1.002
AlSb	6.135 8	2.3	2.21	1.612	0.47
GaP	5.451 0	2.78	2.6	2.272	0.797
GaAs	5.653 25	1.424	1.708	1.900	0.562
GaSb	6.096 02	0.725	0.810	1.032	0.07
InP	5.868 9	1.350	1.95	2.15	0.857
InAs	6.058 3	0.355	1.43[a]	2.0[a]	0.58
InSb	6.479 43	0.170	1.0[a]	1.7	0.04
Si	5.431 1	4.1	2.0	1.124	0.447
Ge	5.657 9	0.805	0.666	0.89	0.072

[a] indicates theoretical estimate

Table 3. Effective masses of electrons in the conduction band minimum and corresponding electron mobilities for a number of compound semiconductors together with their direct energy band gaps.

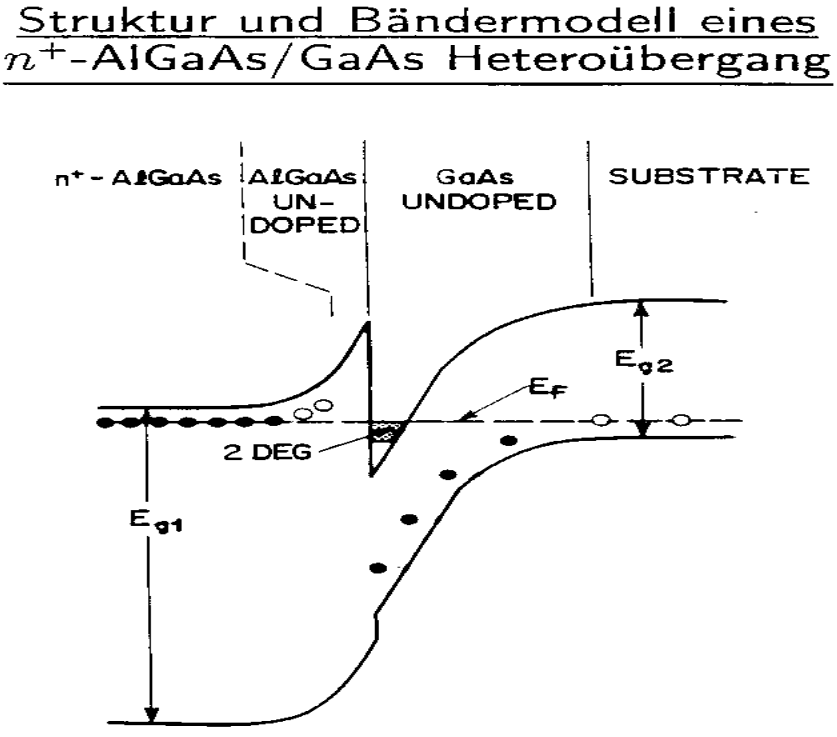

Fig.5. By intentionally doping only the upper part of the AlGaAs layer, a 2DEG without scattering by dopants is obtained.

3) Two-Dimensional Electron-Gas Devices.

By introducing various doping strategies, the electron (or hole) distribution can be set up in accordance with the device requirements. The best-known example is here that of the HEMT (the High Electron Mobility Transistor). The original realization was on GaAs-AlGaAs as shown by Fig. 5. Only the upper part of the GaAlAs is doped to such a degree that all the mobile electrons produced in this way tunnel via the narrow undoped AlGaAs layer into the GaAs, where they accumulate near the AlGaAs and form there a 2DEG (Two-Dimensional Electron Gas). The particular feature of a 2DEG is, that the mobile electrons are separated from the donors so that they are not scattered by them. This produces the highest mobility of electron transport along a 2DEG and thus also the lowest noise figure possible. An example of an integrated circuit as fabricated in Darmstadt is given by Fig. 6.

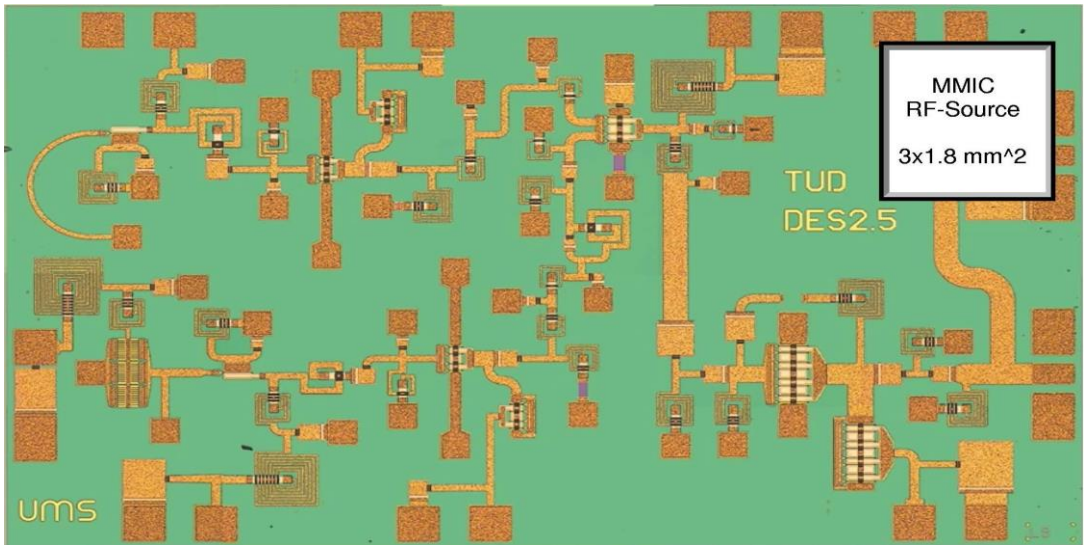

Fig 6 Example of an integrated circuit with HEMTs.

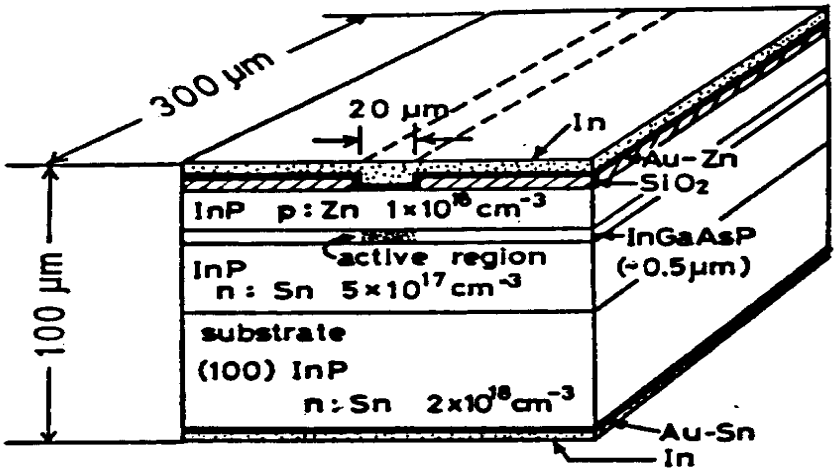

Schematic diagram of an oxide-stripe laser diode for CW operation.

Fig. 7. Schematical diagram of an oxide-stripe laser diode for CW operation**.**

4) The Heterojunction Laser

In order to focus emitted photons back into the photon-generation region, in view to reducing the threshold for lasing with relatively low currents, heterostructures were employed, since each of the epitaxial materials have different optical properties such as the refractive index. An early example of such a laser was that of Fig 7. A more modern example is the laser of Fig. 8 based on nitrides. The particular advantage is there that a wider range of energy gaps is available so that also blue light can be produced und therefore white light emission is possible.

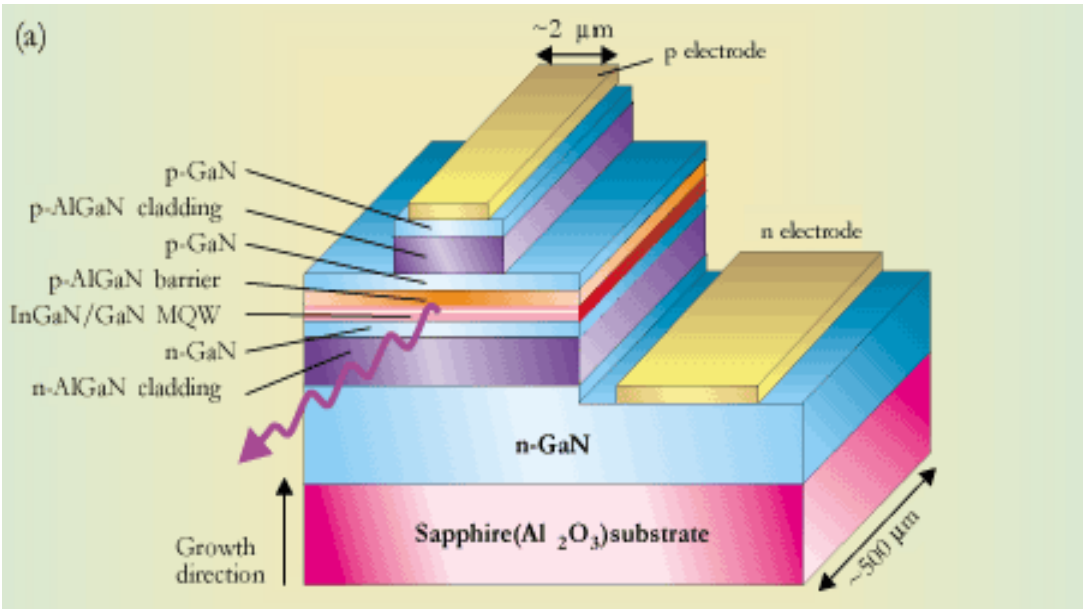

Fig 8. A heterojunction laser with nitrides, grown on Sapphire with an acceptable lattice mismatch**.**

A particularly interesting laser is the quantum cascade laser of Fig 9, which does not operate across the energy gap, but which works only in the conduction band.

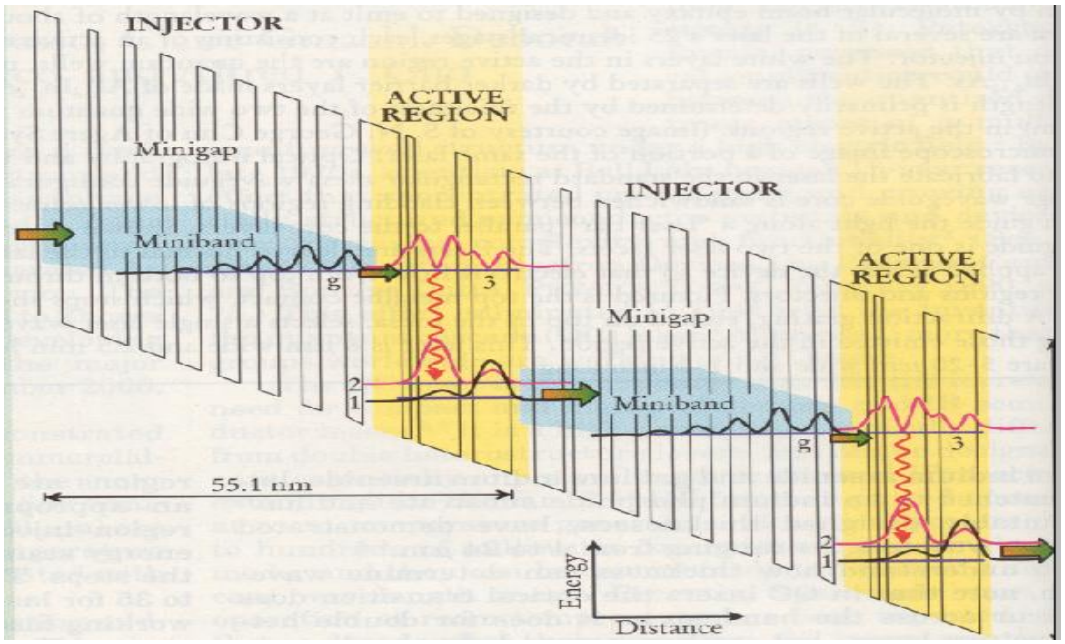

Fig. 9. QCL (Capasso et al) for ~ 60 THz (to avoid thermal excitation out of wells, and bandgap transistions; for population inversion, optical-phonon energies equal or smaller than electron-energy separation, here state separation between 1 and 2 equals phonon energy to remove electrons quickly from state 2)

5) New Nanometric Opportunities.

Semiconductor nanowires (NWs) and 1-Dimensional Electron Gas (1DEG) structures have been widely studied as nanoscale building blocks for nanoelectronics, since they can function both as devices and wires that access the devices. Both types of quantum structures together with some possible components, several ballistic devices, and quantum-dot concepts are reviewed now in this lecture.

NWs are possible directly, as shown above by section 3, by special growth of various materials, such as CdS, ZnS, GaN , Si, Ge , InP etc. . They have been assembled as field-effect transistors (FETs) , inverters , photodetectors , nanosensors , light-emitting diodes and lasers , decoder , non-volatile memory and programmable logic .

Simulations have been done to study the structures, electron spectra, and transport properties of Si nanowires (SiNWs) . Thermal conductivity and optical properties of SiNWs have also been studied. From an applications point of view, it has been shown that doped p type and n type SiNWs can be assembled to form p-n junctions, bipolar transistors, and complementary inverters. These results have lead to the suggestion that SiNWs may become crucial components for nanoscale electronics. The electronic properties of SiNWs such as the band gap, valley splitting, and effective masses as functions of wire dimensions have been studied. The parameters are relevant for the performance of ultrascaled FETs built with SiNWs. An increased bandgap exponentially suppresses parasitic interband tunnelling which is a limit to scaling of Si FETs . For a wire grown in a [100] direction, valley splitting in the conduction band pushes up the two electron valleys aligned along the axis of the wire which reduces the effective mobility mass in the transport direction. Quantum confinement pushes up the conduction band minimum. This results in a transverse mass increased by about 35% for 2.5-nm-thick wires. The corresponding hole masses are increased by a factor of about six. The effective mass affects both the mobility and the density of states. Even for ultrascaled FETs, there are indications that mobility will still be a relevant parameter governing performance. The density of states directly enters into the quantum capacitance and current drive which also affects the performance of ultrascaled FETs.

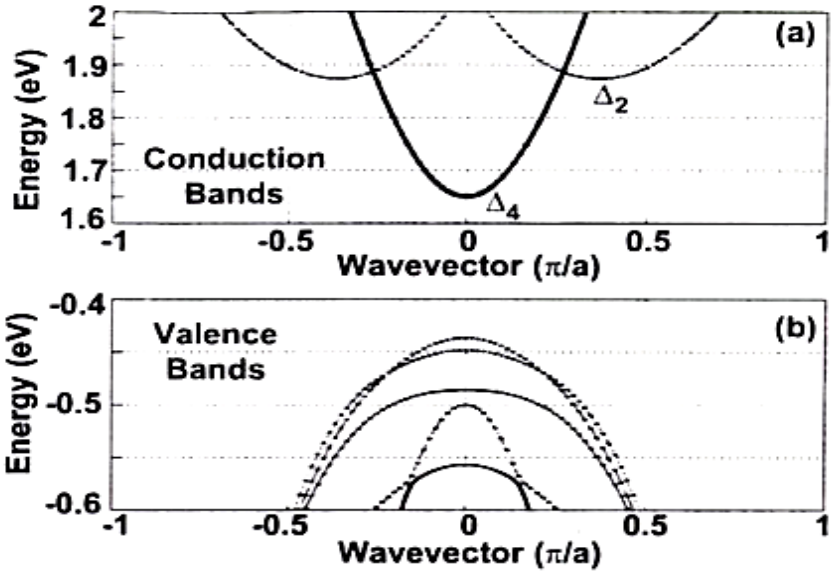

Fig. 10. Si 1.54 x 1.54-nm NW band structure calculated from an empirical tight-binding model.
(a) Conduction bands and
(b) valence bands. The lattice constant a = 5.4 Å.

Fig. 10 shows a typical energy versus wave vector relation for a Si NW. In this case, the NW is 1.54-nm square . The conduction band edge at Γ in the one dimensional (1-D) Brillouin zone is formed from the four equivalent Δ valleys of the bulk Si, and it is therefore labelled Δ_4 in the figure. The next higher valleys are formed from the two equivalent Δ valleys (Δ_2) which point along the vertical [001] axis of the Si wire. The 1-D Brillouin zone of the Si wire is ½ as long as the length of the bulk Si Brillouin zone along the Δ line. In real space, the 1-D Si [001] wire primitive unit cell consists of four atomic layers, whereas the bulk 3-D Si primitive unit cell consists of two Si atoms. The position in the 1-D Brillouin zone of the Δ_2 valley minimums at 0.37 π/α can be qualitatively understood in terms of zone folding. The Δ_2 valley minimum which in bulk Si occurs at 0.81 $2\pi/a$.

In the valence band, there is significant mixing and splitting of the hole bands. The bandgap is increased by quantum confinement. For reference, for bulk Si, the valence band edge is at E = 0 and the conduction band edge is at E = 1.1.3 eV. In the 1-D Brillouin zone of a wire, Si is a direct gap material.

It is possible to produce a number of quantum-mechanical electronic concepts which go well beyond the field-effect transistor. An interesting example is the ballistic conductance quantization measured , as shown by Fig. 11b for the structure of Fig. 11a.. The lower the temperature, the sharper are the steps. Also, the higher the mobility of a material is the higher the temperature when the stepping disappears.

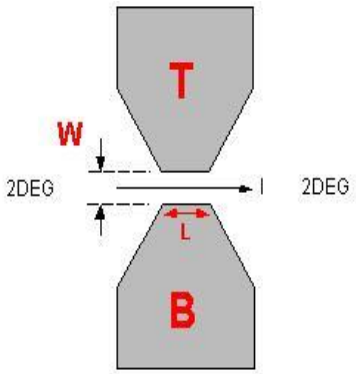

11a) Schematic Drawing of a Quantum Point Contact (QPC) or an Electron Waveguide.

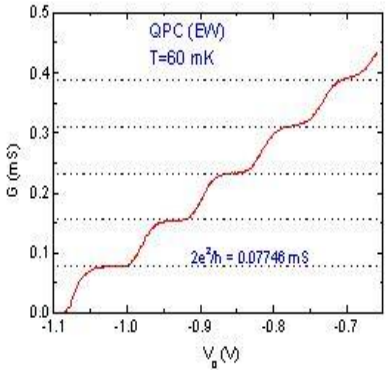

11b) Ballistic Conductance Quantization in a QPC.
L=150 nm and
W=20 nm.

Fig. 11. V_g changes the width of the electronic wave causing 1D subband bottoms to sweep across Fermi level. This results in a quantized conductance

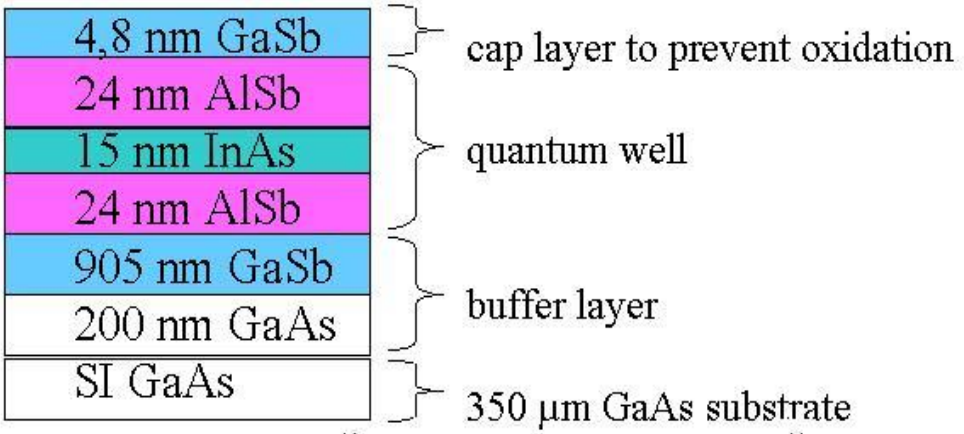

Fig. 12, Layer design of InAs QW wafer grown by MBE

Since this is particularly pronounced with InAs layers, we have been grown these, as shown by Fig. 12.

6) Carbon Nanotubes and Graphene

It is possible to generate EW structures by linking Carbon atoms in a rolled-up one-atomic sheet called graphene. In this way one can develop here quantum-electronic devices.

Carbon nanotubes (CNTs) reveal extraordinary physical properties, which cannot be encountered in any other materials making them extremely attractive for many applications in the area of nanoelectronics. The microwave applications of the CNTs encompass many concepts such as microelectromechanical systems (MEMS), nanoelectromechanical systems (NEMS), field emission, quantum confined electron devices as well as electromagnetic field propagation phenomena in the range 1 GHz-3 THz. In the most of the cases, a microwave device based CNT is a combination of some above concepts.

CNTs are void cylinders realized by rolling a single or several concentric two-dimesional layers of graphite atoms. The single layer formed by graphite atoms, is termed as graphene, displaying a two-dimensional honeycomb structure of sp2 carbon atoms. Single-walled carbon nanotube (SWCNT) displayed in Fig. 13 a is the nanotube realized by rolling a single graphene layer. The multi-walled carbon nanotube (MWCNT) is obtained by rolling several concentric graphene layers. The physical properties of SWCNTs and MWCNTs are many times very different, and always the type of CNT involved in a certain application must be carefully chosen. Depending on how the graphene layer (or layers) is (are) rolled we can get carbon nanotubes (CNTs) with metallic or a semiconducting behavior

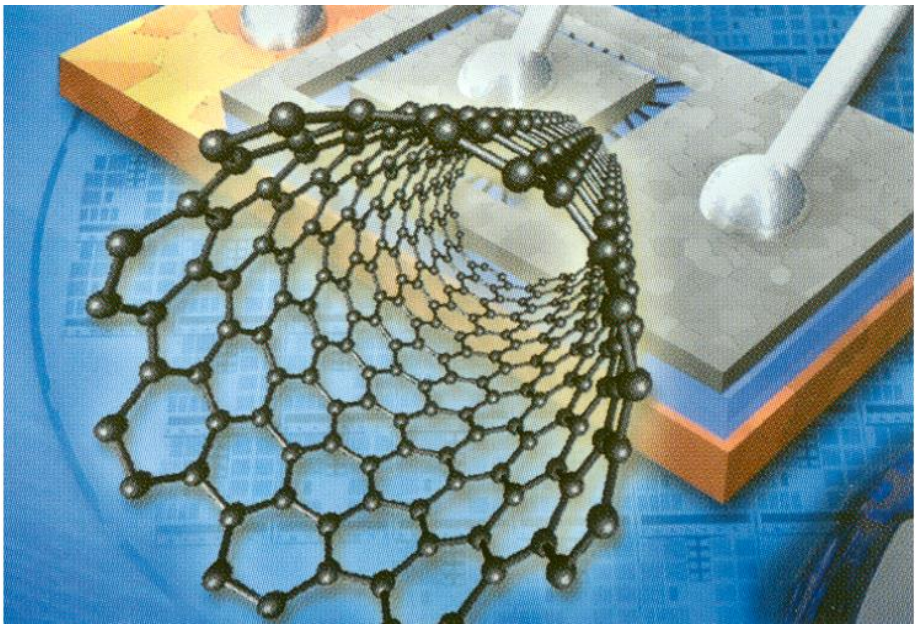

Figure 13. Carbon Nano-Tube, artist-drawn onto simple FET structure (Company Siemens, Germany)

Thus, if the graphene sheets is folded with different orientations it is possible to tailor the fundamental material properties of CNTs. This ability is unique among any known material.

The CNT can be metallic or the semiconducting in character .

CNTs can be functionalized in many ways:

- by doping,
- individual atoms,
- by radial mechanical deformations,
- by application of external or magnetic fields.

In the following a selection of the high frequency devices are briefly indicated, ranging from RF up to THz based on cabon nanotubes. Some of them were expermentally tested others are only designed and simulated. However, all of them have something in common irrespective of the bandwidth in which they are working. They are all tunable, because the electrical properties of the CNTs are inherently tunable. Field-emission devices are based on the emission of electrons into vacuum due to a very high local electric field. If the thickness of this barrier is only a few nm, the electrons tunnel from the highest occupied states in the solid into the vacuum and then travel ballistically in the vacuum without any scattering.

There are various high-frequency passive and active devices based on carbon nanotubes envisaged. The electromagnetic properties of the CNT films have been investigated in the range up to 3THz regarding antireflection, electrostatic protection and electromagnetic interference shielding. The utilization of CNT films as a high-loss nanomaterial as a high-performance radar-absorbent material (RAM) is very promising according to present experiments.

Graphen eis a material of great excitement with microwave transistors realized experimentally by a number of industrial companies. Large scale grapheme sheets do not have a band gap and is a semimetal with charge carriers of zero mass at the Dirac point. (See Fig 14) A band gap can be formed by confinement in nano-ribbon or nano-constriction structures. For example, the induced bandgap by a 50 nm wide nanoribbon is about 6 meV, a 30 nm constriction width result in about 14 meV. The charge carrier mass then increases, but is still very small. The energy gap of graphene stripes is similar to that of Carbon NanoTubes (CNT), whose value is E_G (eV)=0.8/d(/nm) (d = CNT diameter). To obtain a ballistic graphene resonator, we propose the following structure: narrow width - large width - narrow width (Fig. 15). The usual approach is to use monolayer grapheme.

It is possible to consider the designs of a variety of semiconducting graphene structures where electrons (and holes) are heated appropriately by suitable stripe structures under the action of applied voltages, similarly to the quantum cascade laser of Fig.9. These electrons enter then a resonance region with two states. By dropping from the higher energy state to the lower one, energy of a THz photon is lost and the corresponding photon can be emitted. With an external resonator a laser can be realized, where the graphene nanostructures acts as active medium. Similarly, non-linear mixers are proposed for THz applications.

Fig. 14, Energy Contours of Graphene in Momentum Space (Semi-Metal for infinite sheet)

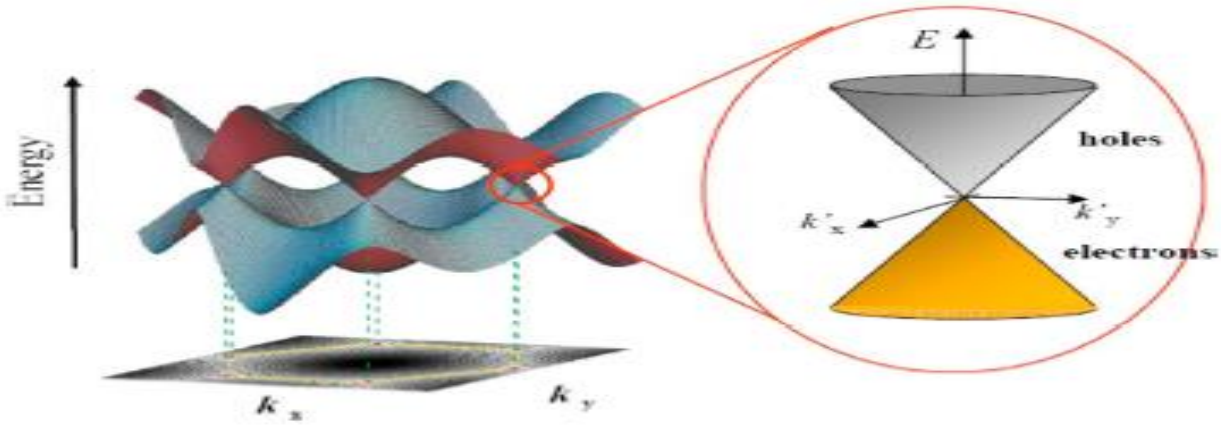

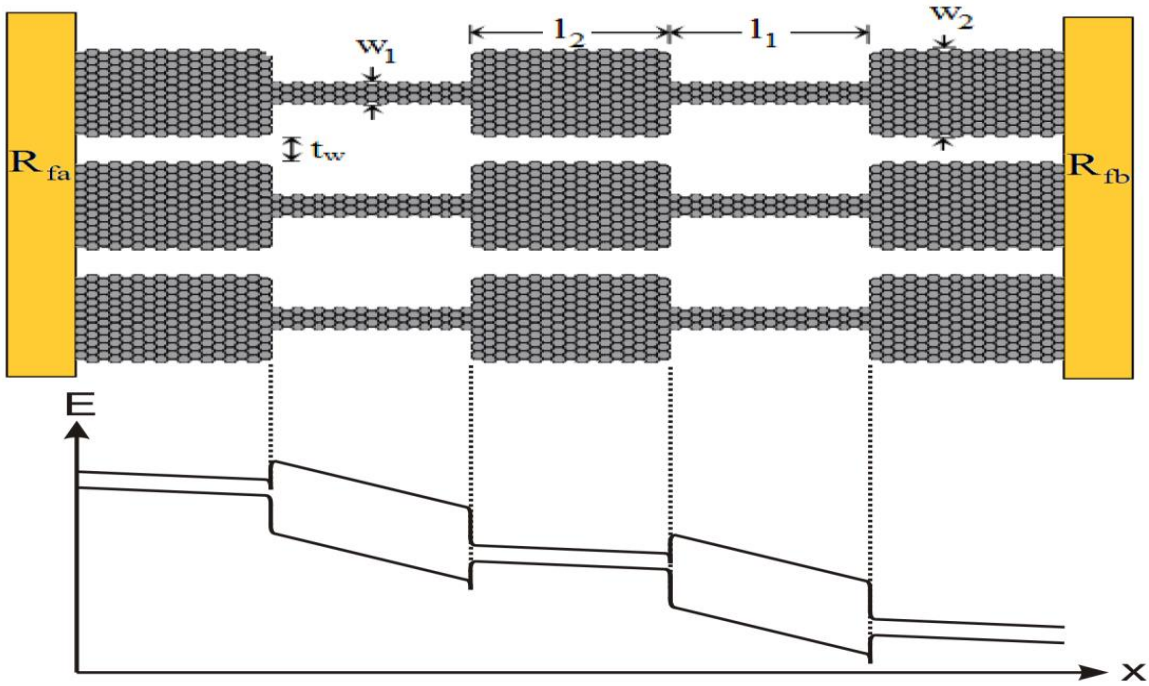

Fig 15. Real space (top) and band diagram (bottom) under bias for a ballistic graphene resonator structure. The design data are: G_1 = 200 meV, and G_2= 40 meV, w_1 = 17 nm, and w_2 = 21 nm, $l_2 = v_0 / f$, $v_0 \approx v_F \approx 10^6$ m/s , v_0 the electron velocity, v_F the Fermi velocity in graphene [8], f=Terahertz frequency; for f = 1 THz : l_2 = 1 µm, $l_1 = t_w \approx l_2 / 3$.

7) An Electron-Wave Resonator for the generation of THz signals

There are numerous approaches to generate relatively acceptable power levels in the frequency range up to 2 THz, but none is satisfactory regarding low cost, reasonable efficiency and small size and weight. Here the development of a totally new type of device is described which possibly represents an answer to this problem.

The new concept is based on room-temperature reflection of ballistic electrons in a short (length L typically 150 nm) high-mobility n-type semiconductor terminated at both ends by wide band gap materials as shown for a simple example in Fig. 16. The length L is sufficiently short for ballistic electron resonance to occur at room temperature. The reflection occurs at the edge of the heterojunctions without any loss of kinetic energy. The electrons are accelerated towards the barrier by an energizing RF voltage Ve, of sinusoidal or pulse-shape. The electrons are reflected several times with gradual loss of energy due to occasional scattering. They then need to be accelerated again by the opposite phase of the voltage of Ve. The material to be selected needs to exhibit good ballistic properties and InGaAs was used for a first experimental realization, although there are possibly also still better materials.

The device is called: Ballistic Electron Wave Swing (BEWAS). Monte Carlo simulation has shown that this device gives a good efficiency of a suitably designed 1 THz device. This device is not a harmonic generator for Ve (say the 100 GHz input), but generates the THz signal by electron resonance. The device is therefore an electron wave device which can be considered to be equivalent to the electromagnetic wave resonator, i.e. the well known laser. The energy is provided by the applied Ve.

A semi-classical self-consistent ensemble Monte Carlo (MC) model is used to simulate the electron dynamic in the In0.52Al0.48As/In0.53Ga0.47As/In0.52Al0.48As double-hetero-

junction structures. The band offset between the Γ-valleys of In0.52Al0.48As and In0.53Ga0.47As is taken as 0.5 eV. This ensemble MC simulator is self-consistently coupled with a Poisson solver, where the potential profile between the contact layers was derived at a time step of 1 fs. The Poisson equation was solved on a uniform spatial mesh with spacing of 1 nm. In the model, abrupt heterojunctions are assumed and the interface perfectly reflects the impinging electron, where its wave vector component kz, normal to the interface, is changed to – kz. The electric field in the heavily doped contact layers was assumed falling abruptly to zero at the contact-barrier interface where electrons are in thermal equilibrium with the lattice.

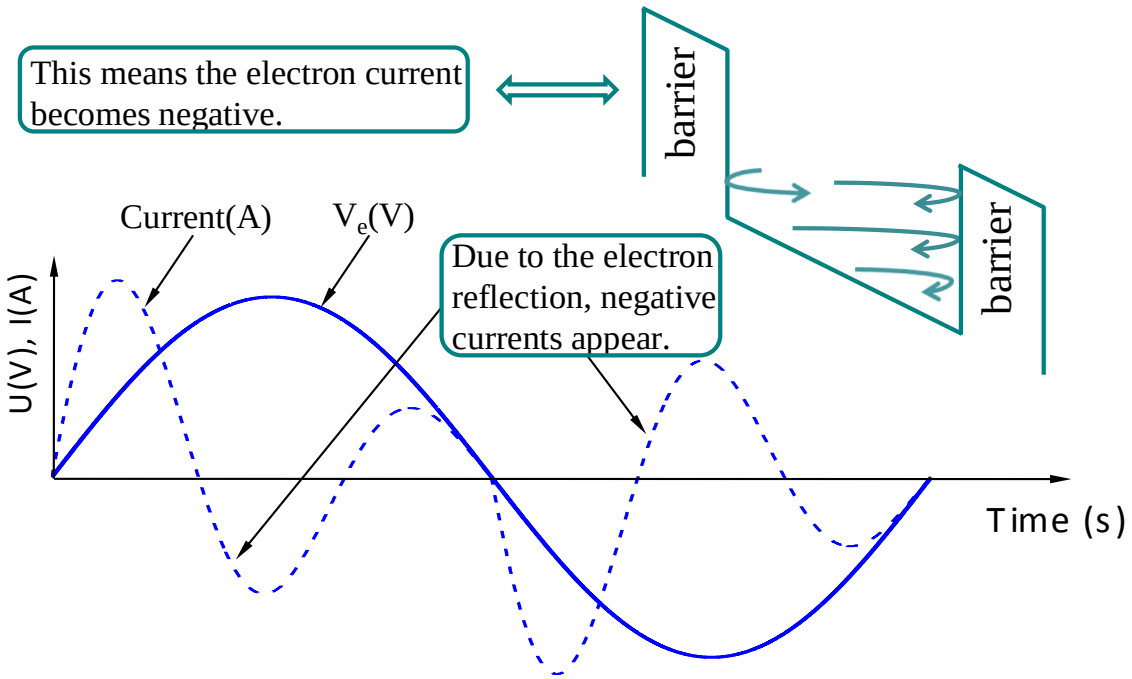

Fig. 16. Variation of the output signal current as function of time for an input RF voltage Ve of very high frequency as selected for a verification of the concept proposed.

The large positive and negative mean electron velocities recorded in the well at both positive and negative peak biases confirmed that electrons in the well travel quasi-ballistically to reach such high speeds before being reflected from the heterointerfaces.

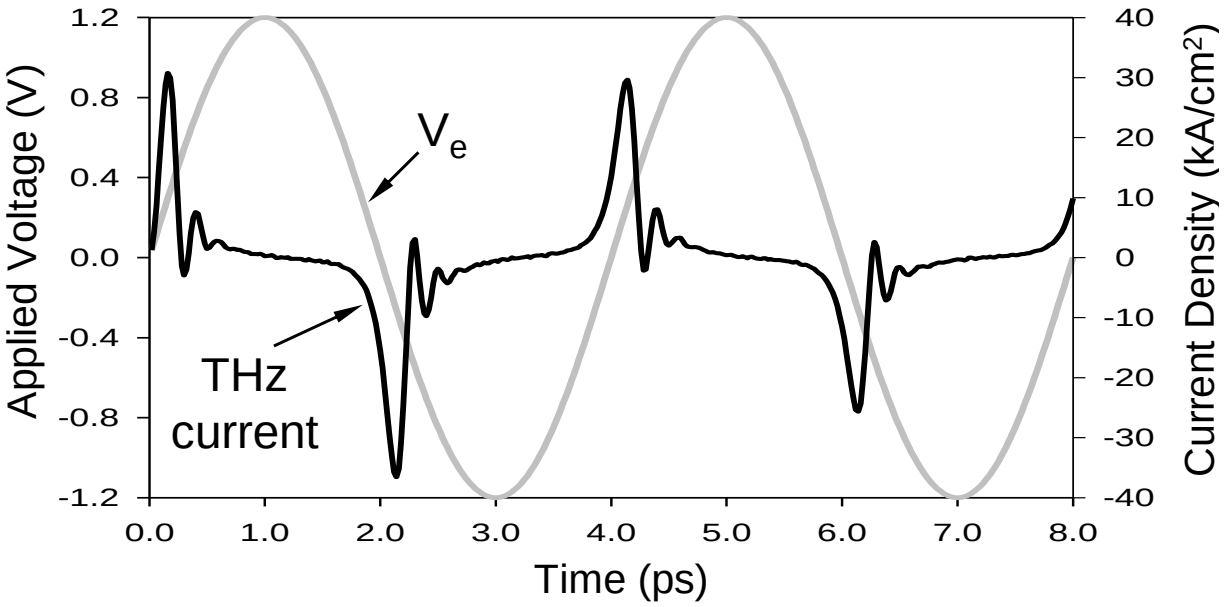

Fig. 17. Temporal evolution of current density in response to sinusoidal signal.

The first experimental confirmation by Mr. I. Oprea is based on an epitaxial sandwich with two barriers and an InGaAs well with a doping concentration of 1.5 x 1016 and a width of 144 nm as given by Fig. 18 (a). The experimental setup is based on Fig. 18 (b), where a 3-D computer model of the fabricated structure is shown. The total chip dimensions of the fabricated structure are 280 μm (l) x 80 μm (W) x 80 μm (H). The device fabrication was based on optical lithography with TiPtAu ohmic contacts deposited on the highly doped top InGaAs layer. The bottom contact layer was used to interconnect two device structures in opposition, where each of the devices has the top contacts connected to striplines via airbridges. The structurization was done by PR-masking and a wet etchant H3PO4/H2O2/H2O.

(a)

Layer	Thickness(nm)	Doping(cm^{-3})
n^{++}-$In_{0.53}Ga_{0.47}As$ contact	150	$1x10^{19}$
$In_{0.52}Al_{0.48}As$ barrier	15	undoped
$In_{0.53}Ga_{0.47}As$ spacer	3	undoped
n^{+} - $In_{0.53}Ga_{0.47}As$	144	$1.5x10^{16}$
$In_{0.53}Ga_{0.47}As$ spacer	3	undoped
$In_{0.52}Al_{0.48}A$ barrier	15	undoped
n^{++}-$In_{0.53}Ga_{0.47}As$ contact	2000	$1x10^{19}$
InP substrate S.I.		

(b)

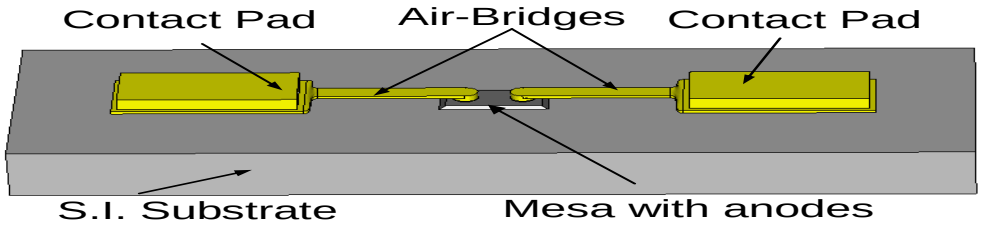

Fig. 18. (a) Epitaxial layers of the wafer used and (b) 3D model of the test structure employed.